Shake-Table Tests of a Full-Scale Three-Story Reinforced Masonry Shear Wall Structure

A. Stavridis[1]; F. Ahmadi[2]; M. Mavros[3]; P. B. Shing[4]; R. E. Klingner[5]; and D. McLean[6]

Abstract: This paper presents the shake-table tests of a full-scale, 3-story, reinforced concrete masonry structure. The structure was a special reinforced masonry shear wall system designed according to current code provisions for an area of high seismicity. It consisted of three lines of walls arranged in an H-shape in plan view, with one lineal and two T-walls aligned in the direction of the table motion and four lineal walls oriented perpendicular to the table motion. The seven walls were separated by door openings and were connected with lintels and precast slabs with cast-in-place concrete topping. The structure was subjected to a series of dynamic tests including nine seismic excitations with intensities exceeding the maximum considered earthquake used in the design. The structure had a capacity that exceeded considerably the design base shear, and it withstood all but the last two excitations with little or no damage. The paper presents the design of the test structure, its dynamic response to the seismic excitations, the evolution of damage, and the major observations and findings from the tests, including the influence of the concrete slabs, lintels, location of lap splices, and walls oriented perpendicular to the direction of the table motion on the structural performance. **DOI: 10.1061/(ASCE)ST.1943-541X.0001527.**

Author keywords: Concrete and masonry structures.

Introduction

Strength design has been increasingly used to design reinforced masonry structures. In the United States, the transition from allowable-stress design (which is still permitted by the 2013 MSJC Code) to strength design was largely facilitated by the research program carried out by the Technical Coordinating Committee for Masonry Research (TCCMAR) (Bozorgnia and Bertero 2004). In that program, researchers examined the basic stress-block parameters used to estimate the flexural strength of reinforced masonry walls and beams (Assis et al. 1989), validated basic design principles for flexure-dominated and shear-dominated masonry shear-wall segments (Shing et al. 1990), studied the seismic behavior and design of low-rise masonry shear wall structures with openings (Leiva and Klingner 1994), and investigated the effective flange width for T-wall segments (Priestley 1993). The performance of wall systems was studied through shake-table tests of two quarter-scale, 3-story, building specimens (Abrams and Paulson 1991) and pseudo-dynamic tests of a full-scale, five-story, reinforced masonry structure (Seible et al. 1994a, b). Besides the TCCMAR program, shake-table tests were conducted on small-scale specimens (Gulkan et al. 1990a, b; Cohen 2004a, b; Mojiri et al. 2014) and on a full-scale, single-story, concrete masonry building with brick veneer (Klingner et al. 2010). These tests have indicated that reinforced masonry structures can perform well under seismic loads.

However, the behavior of a reinforced masonry structure investigated in a laboratory is sensitive to the scale of the structural specimen, the rate-of-loading effects, and the distribution of the lateral seismic forces along the height of the structure in the case of a multi-story specimen. Moreover, it can be affected by the applied boundary conditions, which may not properly account for the interaction of different components in the system. Due to these complexities, there is still much to be understood about the seismic performance of multi-story reinforced masonry shear-wall systems, including the influence of floor diaphragms, lap splices in the walls, and walls loaded out-of-plane on the seismic response of a wall system. Because of this lack of understanding, requirements in different building codes may not necessarily be consistent. For instance, ASCE 7-05 and Eurocode EC6 (2005) do not allow reinforcing steel to have lap splices in plastic-hinge regions of wall components, while the New Zealand Standard NZS 4230 (2004) and TMS 402-13 (MSJC 2013) permit their use even though the former discourages it and requires 50% longer splices if those are in a plastic hinge region. Hence, additional data are needed to determine the adequacy of current design provisions and to calibrate and validate computational models (e.g., Ahmadi 2012; Sayah et al. 2013), which can be used for the performance-based design and seismic performance assessment of these structures.

This paper presents the tests of a full-scale, 3-story, reinforced masonry structure conducted on the outdoor shake table at the University of California, San Diego (UCSD). The test structure represented a typical module of a building. It consisted of special reinforced masonry shear walls designed according to ASCE/SEI 7-05 (ASCE/SEI 2005) and TMS 402-08 (MSJC 2008) and was built with reinforcing details, materials, and construction practices representative of modern construction in an area of high seismic

[1]Assistant Professor, Dept. of Civil, Structural and Environmental Engineering, Univ. at Buffalo, Buffalo, NY 14260 (corresponding author).
[2]Postdoctoral Researcher, Dept. of Civil Engineering, Univ. of Texas, Austin, TX 78712.
[3]Ph.D. Student, Dept. of Structural Engineering, Univ. of California, San Diego, La Jolla, CA 92093.
[4]Professor, Dept. of Structural Engineering, Univ. of California, San Diego, La Jolla, CA 92093.
[5]Professor Emeritus, Dept. of Civil Engineering, Univ. of Texas, Austin, TX 78712.
[6]Professor and Dean of Engineering, Dept. of Civil and Environmental Engineering, Colorado State Univ., Fort Collins, CO 80523.

Note. This manuscript was submitted on January 23, 2015; approved on February 2, 2016No Epub Date. Discussion period open until 0, 0; separate discussions must be submitted for individual papers. This paper is part of the ***Journal of Structural Engineering***, © ASCE, ISSN 0733-9445.

hazard in California. It was subjected to a sequence of 14 uniaxial earthquake records scaled to different intensity levels. The paper presents the major findings of this study and discusses their implications for design.

Prototype Structure and Specimen Design

Prototype Building and Test Structure Layout

The prototype structure considered in this study was a 3-story reinforced masonry shear-wall building with a configuration representative of an apartment or office building. It consisted of repeated modules of shear walls designed to carry the gravity and seismic loads. The test structure, shown in Fig. 1, represented a segment of the prototype building. It was symmetric and rectangular in plan, with dimensions of 7.3 m (24 ft) in the direction of shaking, and 6.3 m (20.67 ft.) perpendicular to the direction of shaking. The structural system consisted of five lineal walls with rectangular sections and two T-walls. The walls, shown in Fig. 1(a), are named W-1 through W-9. The naming scheme used here differentiates between the web and the flange of the T-walls. Walls W-1, W-2, and W-3, which were parallel to the direction of shaking, are called in-plane walls, while W-4 through W-9 are called out-of-plane walls. As shown in the figure, the T-walls had their webs parallel to the direction of shaking. The roof and floor diaphragms consisted of precast, prestressed, hollow-core planks with cast-in-place concrete topping. The planks were supported on the out-of-plane walls, spanning parallel to Walls W-1, W-2, and W-3.

Test Structure Design

The prototype building was assigned to Seismic Design Category (SDC) D with a seismic hazard level comparable to San Diego, California, and site class D. The design spectral intensities, S_{DS} and S_{D1}, according to ASCE 7-05 (ASCE/SEI 2005) were 1.0 g and 0.6 g, respectively. It had a special reinforced masonry bearing wall system design and was detailed according to TMS 402-08 (MSJC 2008) with a seismic response modification coefficient (R factor) of 5. The structural period for design was calculated to be 0.23 s according to ASCE 7-05. The total seismic weight considered for the test structure was 1,024 kN (230 kips), with 280 kN (62.9 kips), 372 kN (83.6 kips), and 372 kN (83.6 kips) at the roof, third, and second levels, respectively. The resulting design base shear was 203 kN (45.7 kips). It was assumed that the gravity loads from the slabs were carried by Walls W-4 through W-9, which supported the precast planks. The base shear was distributed among the two T-walls and the lineal wall, W-2, in proportion to their elastic uncracked flexural stiffnesses. To simplify the design calculations, the coupling effect of the slabs and lintels was ignored as it is often done in design practice due to uncertainties in the performance of the lintels and the connections between the walls and the slabs (Leiva and Klingner 1994). As a result, the two T-walls and the lineal in-plane wall were assumed to behave as cantilever walls along their entire height. If the effect of coupling was considered, the design moments for the T-walls would have been reduced by 70 to 80% and the prescriptive requirements of TMS 401-08 would have governed the reinforcement detailing.

The vertical reinforcement required for the in-plane walls to resist the seismic loads exceeded the prescriptive requirements of TMS 402-08 for special walls. The horizontal reinforcement was governed by the prescriptive spacing requirement of the code and resulted in a shear capacity that was two times that required to meet the shear capacity design requirement. Walls W-1 and W-5 (comprising the west T-wall), W-2, and W-3 and W-8 (comprising the east T-wall) had a longitudinal reinforcement ratio of 0.0033, while the horizontal reinforcement ratio was 0.0016. For the remaining four out-of-plane walls (W-4, W-6, W-7, and W9), both the vertical and the horizontal reinforcement was selected according to the prescriptive requirements. The vertical and horizontal reinforcement ratios for these walls were 0.0023 and 0.0016, respectively. The materials specified in the design were cement-lime mortar meeting ASTM C270 specifications for Type S by

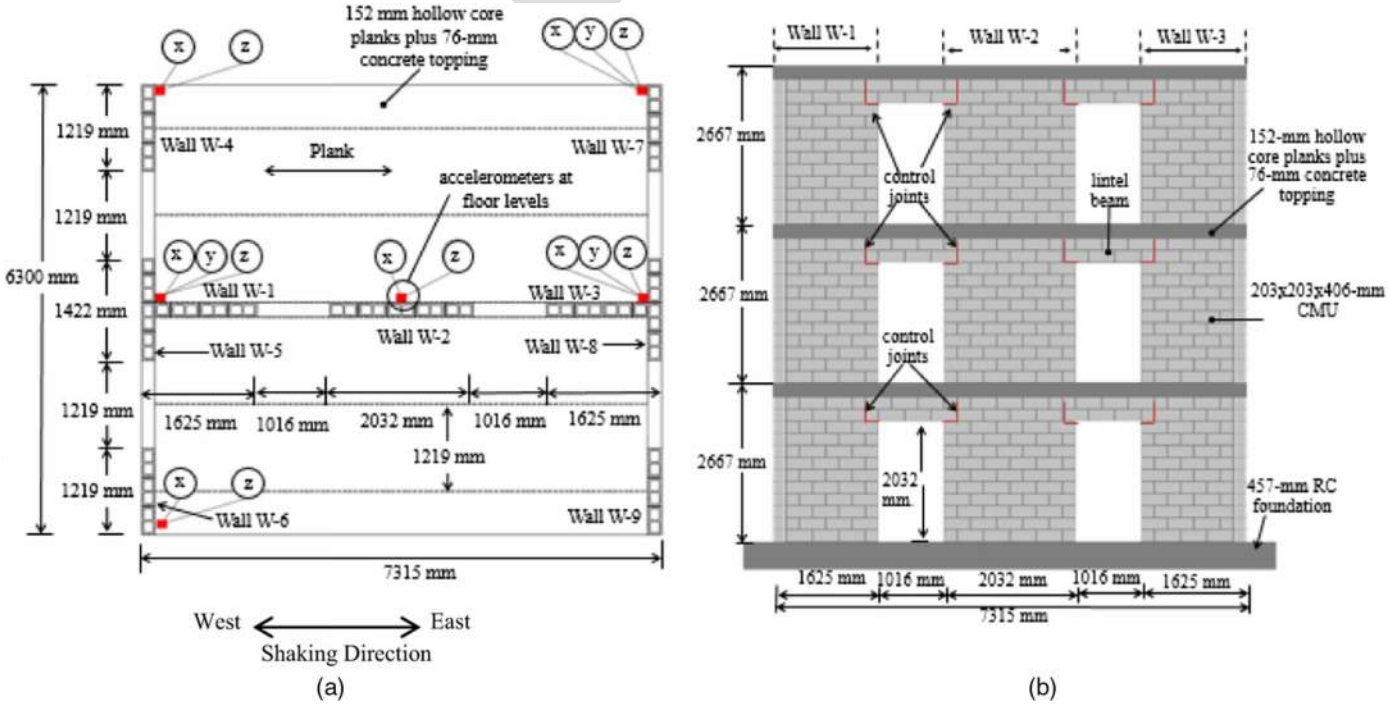

F1:1 **Fig. 1.** Configuration of test structure: (a) plan view of typical floor, wall naming scheme, and locations of accelerometers; (b) elevation view

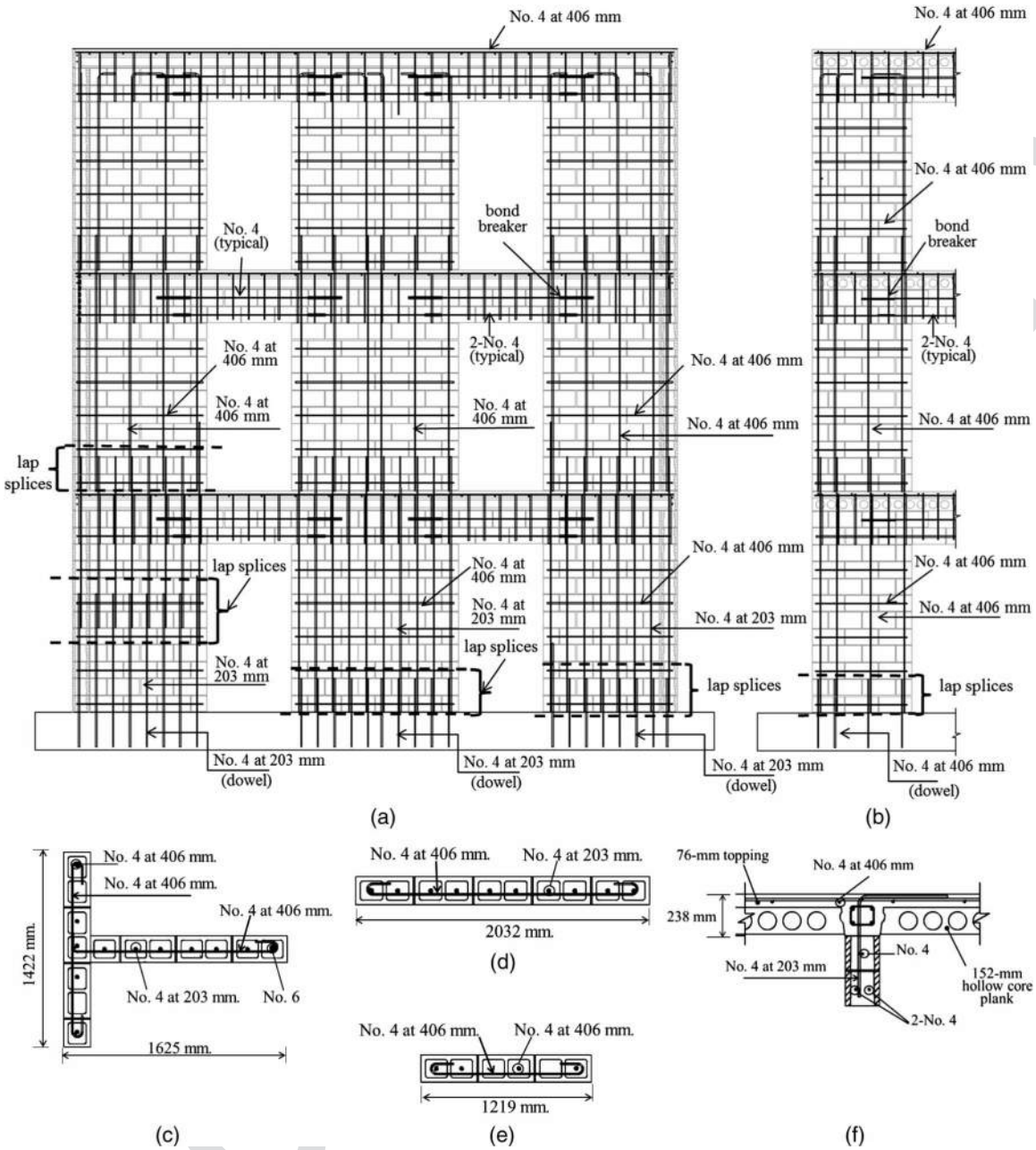

F2:1 **Fig. 2.** Reinforcement details: (a) reinforcement details for walls parallel to the direction of shaking (Walls W-1, W-2, and W-3); (b) typical
F2:2 reinforcement details for out-of-plane walls; (c) T-wall sections; (d) W-2 section; (e) out-of-plane wall sections; and (f) typical cross-sectional details
F2:3 of lintel beams and floor system

proportion, concrete masonry units meeting ASTM C90 with a compressive strength of 17.2 MPa (2.5 ksi), and ASTM A615 Grade 60 steel for the reinforcing bars. The design details for all walls are presented in Fig. 2. Based on the specified material strengths and with the coupling effect of the lintels and horizontal slabs ignored, the flexure-dominated total base shear capacity of the three in-plane walls including the wall flanges is 316 kN (71 kips).

The roof diaphragm consisted of 152 mm (6 in.) thick prestressed concrete planks, spanning parallel to the direction of shaking as shown in Figs. 1(a) and 2(f). The planks were covered by 76 mm (3 in.) of concrete topping and reinforced with No. 4 bars at 406 mm (16 in.) on center in both directions. To ensure the transfer of shear between the floor system and the wall segments and lintel beams, No. 4 bars spaced at 203 mm (8 in.) on center and bent into an L-shape as shown in Fig. 2(f) were used.

The locations of lap splices in the vertical reinforcement are shown in Figs. 2(a and b). Walls W-1 and W-5 had vertical reinforcement in the bottom story spliced at the mid-height of the story, while the rest of the walls and the upper-story segments of W-1 and W-5 had vertical reinforcement spliced at the base of each story, a potential plastic-hinge zone. The former complied with ASCE 7 (2005), which requires lap splices to be away from potential plastic-hinge zones, while the latter was permitted by TMS 402-08 (MSJC 2008). The walls did not have shear keys at their bases. Control joints were introduced on each side of the lintel beams above door openings. The flexural reinforcing bars in the lintels were continued in the walls, but were debonded for the first 300 mm after the

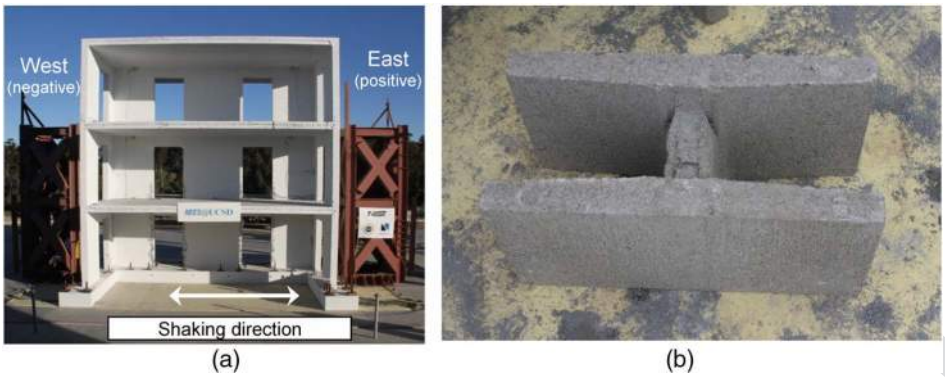

F3:1 **Fig. 3.** Test setup and typical concrete masonry unit: (a) test setup; (b) H-shaped CMU used in construction

control joints, as shown in Figs. 2(a and b), to reduce the coupling moments transmitted to the wall elements. More details about the design of the specimen and the prototype structure are given in Ahmadi (2012).

Test Setup, Material Properties and Instrumentation

Test Structure Construction and Test Setup

The full-scale test structure did not include the loads due to partitions, plumbing, and electrical and mechanical equipment considered in the design. As a result, the seismic weight of the test structure was 923.9 kN (207.7 kips), which is 10% less than the seismic weight of 1,024 kN (230 kips) considered in the design. The use of a smaller mass in the test structure decreased the seismic demand proportionally. It also reduced the axial load on the walls, and thereby reduced their moment and shear capacities by 1 to 2%.

The test setup is shown in Fig. 3(a). Walls W-1, W-2, and W-3 were oriented along the east-west direction, which was the direction of the table motion, as shown in Fig. 1(a). The masonry walls were constructed by professional masons over a period of six weeks. The walls were fully grouted one story at a time. Open-end, H-shaped concrete masonry units (CMUs) with nominal dimensions of 203 × 203 × 406 mm (8 × 8 × 16 in.) were used to facilitate the placement of units around the vertical bars and to enhance the continuity of the grout. A typical unit is shown in Fig. 3(b). Two steel towers were secured on the shake table on the east and west sides of the structure to prevent uncontrolled collapse of the structure on the table. The steel towers were separated from the structure with 610 mm (24-in.) gaps.

Table 1. Average Properties of Reinforcing Steel Bars

Bar number	Nominal diameter [mm (in.)]	Yield stress [MPa (ksi)]	Yield strain $\times 10^{-3}$	Tensile strength [MPa (ksi)]	Strain at fracture
4	12.7 (0.50)	434 (62.9)	2.30	718 (104)	0.172
6	19.1 (0.75)	442 (64.1)	2.29	613 (88.9)	0.196

Material Properties

Tension tests were conducted on samples of reinforcing bars of each size and the results are summarized in Table 1. Compression tests were conducted on 152 × 304 mm (6 × 12 in.) concrete cylinders to obtain the properties of the slab topping, 102 × 203 mm (4 × 8 in.) grout cylinders, 102 × 102 × 194 mm (4 × 4 × 7.625 in.) grout prisms prepared with CMU molds according to ASTM C1019 specifications, 51 × 102 mm (2 × 4 in.) mortar cylinders, 102 × 102 × 194 mm (4 × 4 × 7.625 in.) mortar prisms prepared in a way similar to that for the grout prisms, and 3-unit tall grouted masonry prisms. Split-cylinder tests were conducted on concrete, grout, and mortar specimens. All material samples were obtained from the concrete, grout, and mortar mixes used for the construction of the test structure. The masonry, grout, and mortar prisms were cured outdoors next to the test structure and experienced the same environmental conditions; the concrete, grout, and mortar cylinders were cured in plastic molds. For each batch of concrete, grout, and mortar used in the construction, material tests were conducted on the 28th day after casting; on January 13, 2011, the day the structure was subjected to the design level earthquake, which is considered the first major seismic test, and on February 8th, 2011, the day of the last shake-table test. The average material properties obtained on those dates are summarized in Tables 2–6.

Instrumentation

To measure strains, displacements, and accelerations at various locations on the test structure, 489 sensors were installed, including 266 strain gages, 133 displacement transducers, and 90

Table 2. Average concrete properties obtained from 152 × 304 mm (6 × 12 in.) cylinders.

	28 day	Day of first major test					Day of last test	
Story	Compressive strength [MPa (ksi)]	Age (Days)	Modulus of elasticity [GPa (ksi)]	Compressive strength [MPa (ksi)]	Strain at peak stress (—)	Tensile strength[a] [MPa (ksi)]	Age (Days)	Compressive strength [MPa (ksi)]
1st Story	32.6 (4.72)	76	19.2 (2,778)	33.3 (4.83)	0.0028	2.95 (0.43)	118	35.5 (5.15)
2nd Story	34.9 (5.06)	64	21.6 (3,129)	39.6 (5.75)	0.0029	3.51 (0.51)	112	39.8 (5.77)
3rd Story	34.7 (5.03)	52	—	—	—	—	94	43.2 (6.26)

[a]Obtained from split-cylinder tests.

Table 3. Average Grout Properties Measured on the Day of the First Major Test

Story	102 × 203 mm (4 × 8 in.) Cylinders				102 × 102 × 194 mm (4 × 4 × 7.625 in.) Prisms[a]	
	Modulus of elasticity [GPa (ksi)]	Compressive strength [MPa (ksi)]	Strain at peak stress	Tensile strength[b] [MPa (ksi)]	Compressive strength [MPa (ksi)]	Modulus of elasticity [GPa (ksi)]
1st Story	10.6 (1,535.7)	26.3 (3.82)	0.0051	2.95 (0.43)	27.4 (3.98)	11.0 (1,590.0)
2nd Story	11.4 (1,658.1)	24.4 (3.54)	0.0067	2.63 (0.38)	25.6 (3.71)	8.57 (1,243.6)

[a]Specimens prepared using four CMUs for the mold (ASTM C1019).
[b]Obtained from split-cylinder tests.

Table 4. Average Mortar Properties Measured on the Day of the First Major Test

Story	51 × 102 mm (2 × 4 in.) Cylinders				102 × 102 × 194 mm (4 × 4 × 7.625 in.) Prisms[a]
	Modulus of elasticity [GPa (ksi)]	Compressive strength [MPa (ksi)]	Strain at peak stress (−)	Tensile strength[b] [MPa (ksi)]	Compressive strength [MPa (ksi)]
1st Story	6.86 (995.3)	35.3 (5.11)	0.0065	4.45 (0.65)	42.7 (6.19)
2nd Story	7.54 (1093.4)	33.6 (4.87)	0.0074	4.69 (0.68)	—

[a]Specimens prepared using four CMUs to create the mold.
[b]Obtained from split-cylinder tests.

Table 5. Average Masonry Prism Properties

Story	28 day	Day of first major test				Day of last test	
	Compressive strength [MPa (ksi)]	Age (Days)	Modulus of elasticity [GPa (ksi)]	Compressive strength [MPa (ksi)]	Strain at peak stress (−)	Age (Days)	Compressive strength [MPa (ksi)]
1st Story	17.5 (2.53)	79	12.5 (1,813.0)	21.0 (3.05)	0.0027	121	21.4 (3.10)
2nd Story	17.9 (2.59)	71	11.7 (1,692.1)	18.4 (2.66)	0.0025	113	21.0 (3.05)
3rd Story	15.8 (2.29)	58	—	—	—	100	14.9 (2.16)

Table 6. Ground-Motion Records Used for the Shake-Table Tests

Earthquake	Year	Magnitude	Recording station (component)	PGA (g)	PGV (cm/s)	Duration (s)
Imperial valley	1979	6.5	El centro #5 (140° N)	0.519	46.9	39
Imperial valley	1940	7.0	El centro (N-S)	0.313	29.9	40
Northridge	1994	6.7	Sylmar-O.V. hospital (N-S)	0.843	129.6	40
Northridge	1994	6.7	Rinaldi (228° N)	0.838	166.1	15
Chi Chi	1999	7.6	TCU129 (E-W)	1.01	60.0	70

accelerometers. 15 accelerometers were installed on each horizontal diaphragm, as shown in Fig. 1(a). Accelerometers were also used to measure accelerations at the footing level and the out-of-plane accelerations at the mid-height of Walls W-4 through W-9 in each story. Displacement transducers, including linear potentiometers, string potentiometers, and linear variable differential transformers (LVDT) were used, as shown in Fig. 4, to monitor the shear and flexural deformations of Walls W-1, W-2, and W-3, as well as the curvature along the height of these walls in the first story. Displacement transducers were also installed to measure the potential sliding and uplift of the footing with respect to the table, the sliding and uplift of the base of the first-story walls with respect to the footing and the second-level slab, the opening of the control joints, and the possible relative vertical displacements between the web and the flange of the T-walls. The inter-story drifts were measured with displacement transducers mounted on aluminum reference frames anchored onto the floor slabs. Because the frames had small mass and high stiffness, their deformations under dynamic loading were insignificant compared to the measured inter-story displacements. The reinforcing bars were instrumented with strain gages at critical locations of the walls as shown in Fig. 5(a–c), including the lap-splice regions and the locations where yielding was likely to occur. Additional strain gages were used to monitor strains in the reinforcing bars in the concrete topping of the slab on the second floor near the door openings. Detailed instrumentation plans are given in Stavridis et al. (2013).

Loading Protocol and Structural Periods

The structure was subjected to a series of 14 earthquake ground motion records scaled to different intensity levels as shown in Table 7. The table motion was uniaxial along the east-west direction. The acceleration time histories used in the tests were recorded

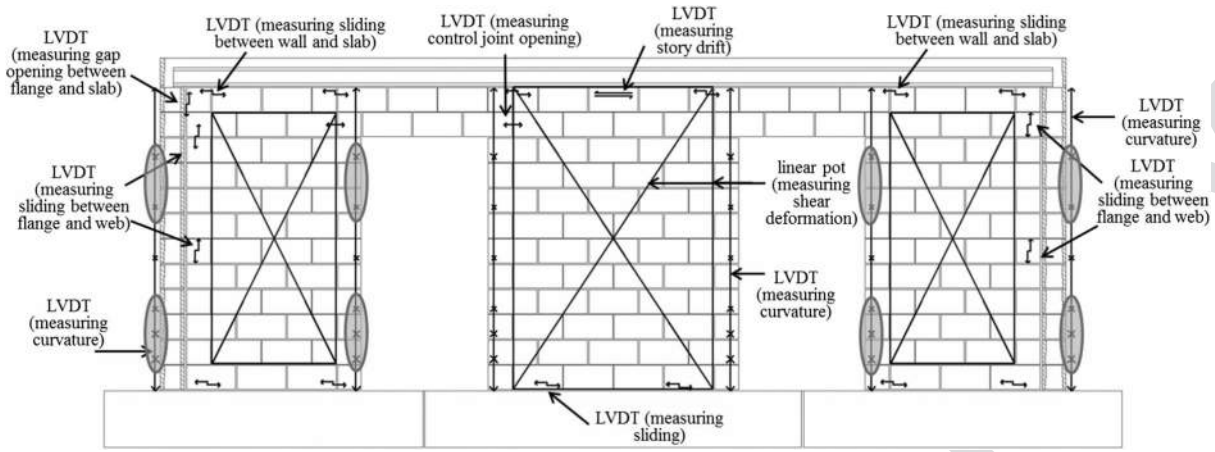

F4:1 **Fig. 4.** Locations of displacement transducers in the first story

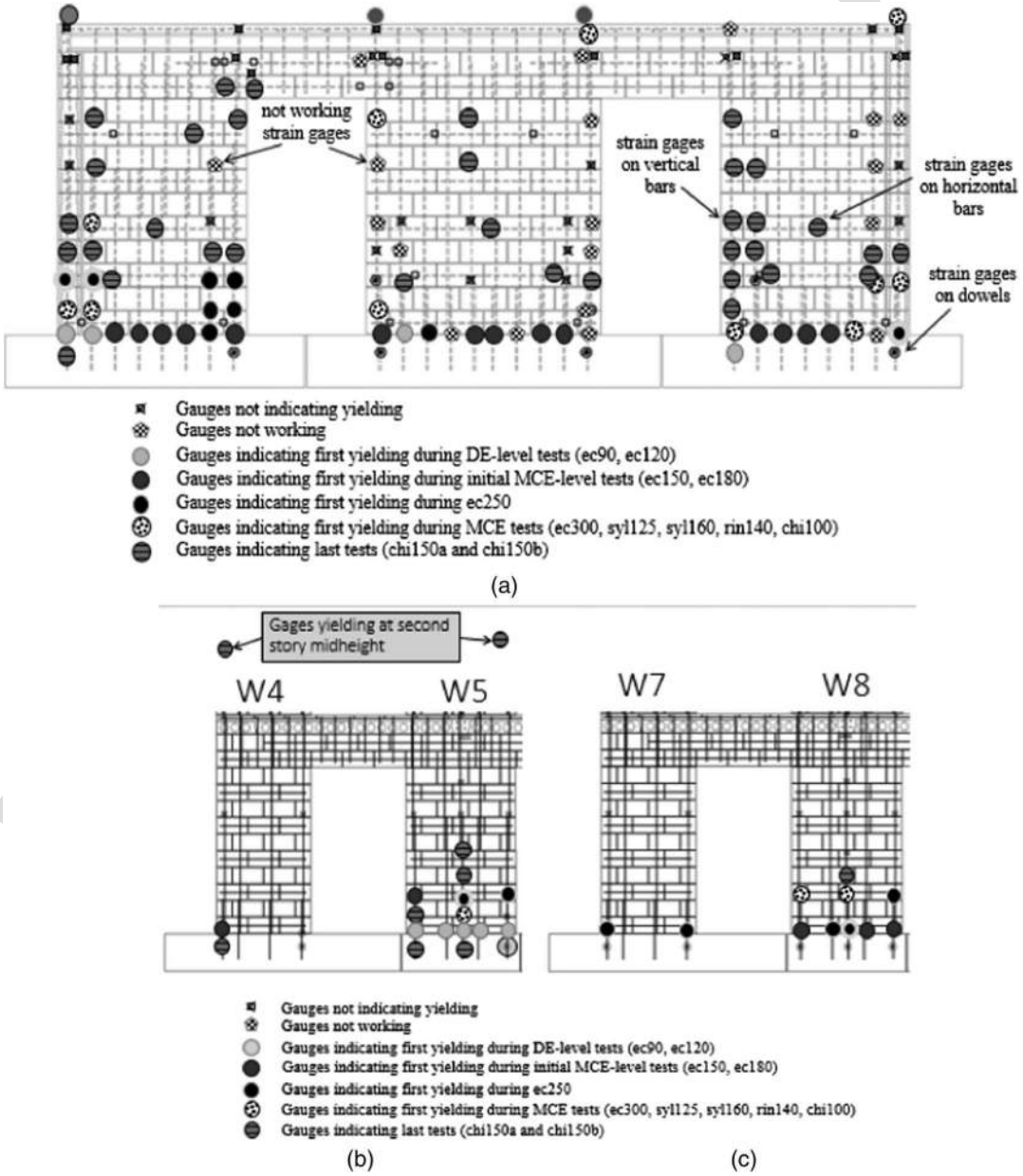

F5:1 **Fig. 5.** Locations of strain gages in the first story: (a) strain gages in W-1, W-2, and W-3; (b) strain gages in W-4 and W-5; and (c) strain gages in W-7
F5:2 and W-8

Table 7. Peak Values of Selected Response Quantities

Test name	Period (T_1) after the test (s)	Effective spectral acceleration scale factor (%)	Intensity factor $R_{Sa} = \text{Avg}[S_a^{REC}/S_a^{MCE}]$	Acceleration		First-story drift (%)	Normalized base shear, V_1/W[a]	Overturning moment (kN-m)	Level of structural damage	W-1 sliding (mm)	W-2 sliding (mm)	W-3 sliding (mm)
				Table	Roof							
ec20	0.09	11.9	0.09	0.10	0.13	—	0.09	483	None	0.0	0.0	0.0
ec45	0.09	31.7	0.25	0.25	0.33	—	0.31	1,495	None	0.0	0.0	0.0
ec90	0.10	71.0	0.60	0.50	0.79	0.04	0.71	3,471	None	0.0	0.1	0.1
ec120	0.11	89.5	0.75	0.64	1.10	0.05	0.97	4,800	Cosmetic	0.1	0.1	0.1
ec150	0.12	131.0	1.03	0.73	1.52	0.09	1.26	6,357	Cosmetic	0.1	0.3	0.2
ec180	0.13	168.0	1.28	0.81	1.80	0.14	1.48	7,350	Cosmetic	0.2	0.7	0.3
ec250	0.19	240.0	1.83	1.11	2.28	0.25	1.73	8,820	Minor	0.8	3.1	0.8
ec300[b]	0.19	194.2	0.83	0.90	1.42	0.14	0.98	4,909	Minor	0.6	2.1	0.7
syl125	0.19	128.8	1.00	1.17	1.68	0.25	1.53	7,253	Minor	1.0	3.6	1.4
syl160	0.21	162.6	1.32	1.56	2.19	0.38	1.90	9,067	Moderate	1.4	5.9	1.8
rin140	0.22	149.7	1.06	1.25	1.75	0.25	1.40	6,604	Moderate	1.4	4.1	1.9
chi100	0.22	113.7	1.32	1.04	2.18	0.36	1.65	8,039	Moderate	2.2	5.9	2.5
chi150a	0.25	137.9	1.96	1.48	2.89	0.74	2.03	9,902	Extensive	3.6	13.5	4.9
chi150b	0.28	122.3	1.52	1.59	2.56	1.59	1.47	8,202	Severe repair	4.7	[c]	5.4

[a]Total weight W of the test specimen was 923.9 kN (207.7 kips).
[b]1940 El Centro.
[c]Sliding exceeded +/− 25.4 mm, the stroke of the instrument.

from the 1940 and 1979 Imperial Valley earthquakes, the 1994 Northridge earthquake, and the 1999 Chi Chi earthquake. These records provide variability in terms of the duration, frequency content, significance of velocity pulses, and spectral accelerations. Table 6 summarizes the main characteristics of the records. The test names shown in the first column of Table 7 contain the abbreviated name of the historical record and the scaling factor in percentage applied to the original record. Fig. 6(a) compares the response spectra, with 5% damping of the unscaled motions to the spectra of the design earthquake (DE) and the maximum considered earthquake (MCE) used in the design. Except for one test (ec300) (the abbreviation ec represents the El Centro #5 record from the 1979 Imperial Valley earthquake), the fundamental period of the intact structure was estimated to be 0.09 s based on a test with white-noise excitation conducted at the beginning of the test series. At this period, a 90% scaling of the amplitude of this record corresponds to the DE intensity based on the spectral acceleration. The records and scaling factors for the subsequent tests were selected based on the fundamental structural period measured before each motion with the goal of applying motions with different characteristics while increasing the seismic demand. Nevertheless, as discussed in the following section, this was not achieved in all cases due to the interaction between the shake table and the test structure.

Ambient-vibration recordings were obtained at the beginning and the end of each test day, and tests with 3-minute white-noise base excitation were conducted before and after each seismic test. The white-noise test data were used to obtain the modal properties of the structure, which would change as damage was induced by the earthquake motions. For the initial tests, the intended white-noise had a root-mean-square (RMS) amplitude of 0.03 g. However, the measured modal properties depend on the amplitude of the base excitation when the structural behavior becomes nonlinear (Yousefianmoghadam et al. 2014). Therefore, once the first cracks appeared after the 180% El Centro test, additional white-noise tests with an RMS amplitude of 0.05 g were also conducted before and after each test.

The fundamental period measured with 0.05 g white noise was greater than that with 0.03 g, especially towards the later stages of the testing sequence when the nonlinearity of the response increased. It was also observed that the white-noise tests conducted at the end of a testing day yielded larger values of the fundamental period than those conducted at the beginning of the subsequent test day. The difference was more noticeable when the two testing days were separated by a longer period of inactivity. For instance, after the 250% El Centro test, the 0.03 and 0.05 g white-noise tests yielded periods of 0.189 and 0.194 s, respectively. At the beginning of the following day, however, the two white-noise tests yielded periods of 0.182 and 0.187 s, respectively. This can be attributed to the autogenous healing of the cementitious materials which occurs in the cracks when uncombined hydrated lime is exposed to air. Table 7 shows the fundamental period of the structure after each earthquake motion test. The values of the fundamental period shown in the table are calculated from results of white-noise tests with 0.03 g RMS amplitude. In all cases, the periods estimated with the two white-noise levels differ by less than 10%.

Intensity of Ground Motions

In shake-table tests, it is useful to relate the structural performance and induced damage to the actual intensity of the excitation. The intensity can be quantified in terms of the spectral

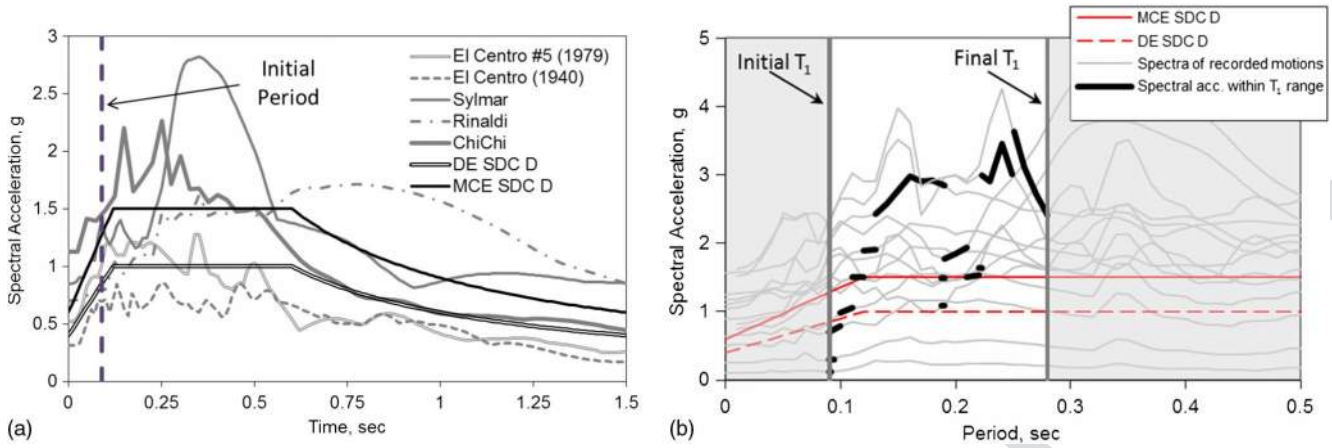

F6:1 F6:2 **Fig. 6.** Acceleration response spectra of unscaled ground motions and actual table motions: (a) response spectra of unscaled ground motions; (b) response spectra of motions recorded on the shake table

314 acceleration of the intended excitation at the fundamental period
315 of the undamaged structure. However, this may not be a mean-
316 ingful measure for the following reasons. First, the output table
317 motion can be different from the intended motion due to the
318 table–structure interaction. Second, the damage induced during a
319 test changes the fundamental period of the structure as shown in
320 Table 7, and thereby changes the dynamic amplification effect.
321 Hence, two intensity indices proposed by Stavridis et al. (2012)
322 are used here to account for the shift of the fundamental period
323 and the discrepancy between the intended and the actual base
324 excitation.

325 The first index, called the effective spectral intensity factor, is
326 the scaling factor that needs to be applied to the original ground
327 motion record so that its average spectral acceleration, calculated
328 over the period range bounded by the fundamental periods of the
329 structure measured just before and after the seismic test, matches
330 that of the motion recorded on the table. The second index com-
331 pares the spectral intensity of each motion to that of the MCE.
332 This index, denoted by R_{Sa}, is defined as the average of the ratio
333 of the spectral acceleration of the table motion to that of the MCE
334 over the period range defined above. The period values defining
335 the period range are estimated from the 0.03 g white-noise tests
336 conducted immediately before and after each test. The use of the
337 0.05 g white-noise tests does not noticeably change the intensity
338 indices.

339 It can be observed from the values of the intensity factor (R_{Sa})
340 presented in Table 7 that although ec90 (90% of the 1979 El Centro
341 motion) was intended to correspond to a design level earthquake,
342 the intended intensity was not attained due to the table-structure
343 interaction. The intensity of the design earthquake was slightly
344 exceeded during ec120, for which $R_{Sa} = 0.75$. The table motion
345 in 9 of the 10 tests after ec120 exceeded the intensity of the MCE.
346 The sole exception was ec300, for which the table motion did not
347 reach the intended intensity. Fig. 6(b) shows the response spectra
348 of the motions recorded on the table. The thick dark lines highlight
349 the spectral intensity of the applied motions for the period ranges
350 bounded by the fundamental periods of the structure measured just
351 before and after each test. The vertical lines at 0.09 and 0.28 s in-
352 dicate the fundamental period at the beginning and at the end of the
353 entire test sequence. The first Chi Chi motion scaled to 150%
354 (chi150a) had the highest spectral intensity; almost twice that of
355 the MCE.

General Test Observations 356

357 For the following discussion of test results, the positive direction is
358 toward the east. Note that walls W-1 and W-4 through W-6 were on
359 the west side of the structure, while W-3 and W-7 through W-9 were
360 on the east side.

Low-Level and DE-Level Tests with 1979 El Centro 361

362 No damage was observed through ec90, which is slightly below the
363 DE according to the intensity ratio (R_{S_a}) shown in Table 7. The next
364 motion, ec120, had a spectral intensity 1.125 times the DE. During
365 this test, the reinforcing bars at the west extreme ends of walls W1
366 and W3 yielded near the base, as shown in Fig. 5(a). Moreover,
367 flexural cracks developed at the control joints above the door open-
368 ings in the first story, as shown in Fig. 7(a). Other than these hair-
369 line cracks, the structure did not sustain any visible damage,
370 although the fundamental period increased from 0.09 to 0.11 s.

MCE Level and Higher-Level Tests with 1979 El Centro 371

372 The structure was subsequently subjected to ec150, ec180, and
373 ec250. As shown in Table 7, the spectral intensity ratios (R_{S_a}) of
374 the base motions in these tests ranged from 1.03 to 1.83, and the
375 first-story drift ratios reached 0.09, 0.14, and 0.25%, respectively.
376 During ec150, some vertical reinforcing bars yielded at the base of
377 the bottom-story Walls W-1, W-2, W-3, and W-5 (the flange of the
378 west T-wall). Considering the locations of the yielded bars shown
379 in Figs. 5(a) and 6(b), one can conclude that the structure was
380 subjected to stronger lateral forces in the east (positive) direction.
381 Horizontal cracks, as shown in Fig. 7(b), developed along the wall-
382 footing interface indicating uplift and sliding of the three in-plane
383 walls. These cracks initiated at the toes of the walls during ec150
384 and propagated during ec180 and ec250. The table motion for
385 ec250 was very demanding, with R_{S_a} equal to 1.83, and caused a
386 significant increase of the fundamental period of the structure from
387 0.13 to 0.19 s. During ec250, fine diagonal cracks appeared in W-1
388 (the web of the west T-wall) as shown in Fig. 7(c), while the base of
389 W-2 slid 3.1 mm (0.12 in.), which was 50% of the total first-story
390 drift and was considerably higher than the sliding measured in
391 the other two in-plane walls (W-1 and W-3). Horizontal cracks
392 also developed in the out-of-plane walls. The elevations of these
393 cracks suggest that they were largely caused by tension due to

F7:1 **Fig. 7.** Initial crack patterns in the first-story walls: (a) cracks at control joints after ec120; (b) shear-sliding cracks at the base (after ec180) and top
F7:2 (after syl125) of W-2; and (c) shear cracks in W-1 after ec250

the overturning moment induced on the test structure. For ec250, the direction of the input acceleration was reversed compared to the previously applied motions of the same record to reduce the directional bias of the input motion. After ec250, most vertical bars had yielded at the base of the bottom-story walls, while the yielding of the four vertical bars at the two extreme sides of Wall W-1, which had splices at its mid height, propagated to the third course. Finally, the two extreme bars of Wall W-2 in the second story also yielded at the wall base during this test.

MCE Level and Above with Other Motions

After the 1979 El Centro motions, the structure was subjected to earthquake records with different spectral characteristics. These included the El Centro record from the 1940 Imperial Valley earthquake, the Rinaldi and Sylmar records from the 1994 Northridge earthquake, which are near-fault ground motions, and a record from the 1999 Chi Chi earthquake in Taiwan, which has a long duration and many cycles of strong shaking. The records were scaled to exceed the MCE level. However, ec300 (300% of the 1940 El Centro) did not achieve the intended intensity due to the table-structure interaction.

During this series of tests, the period of the structure increased from 0.19 to 0.22 s. The most significant change occurred during syl160 (160% of the Sylmar motion), which had a spectral intensity factor (R_{S_a}) of 1.32. The damage to the structure after syl160 was moderate, as shown in Fig. 8. Fine diagonal cracks developed near the top and bottom of Wall W-3 (the web of the east T-wall) as shown in Fig. 8(a), and the diagonal cracks on W-1 propagated. After syl160, all the out-of-plane walls in the first story had horizontal cracks. Moreover, as shown in Fig. 8(e), minor cracks developed in the second story at the control joints near the doors and at the top of W-2. Furthermore, cracks were observed on the slab at the second level near the door openings in the in-plane walls. These cracks initiated near the door openings. After chi100, flexural-shear cracks developed near the bottom of walls W-1 and W-3, and the previously noted cracks propagated further.

During this part of the testing sequence, all the instrumented bars at the base of the in-plane and out-of-plane walls in the bottom and second stories had reached the yield strain. It should be noted

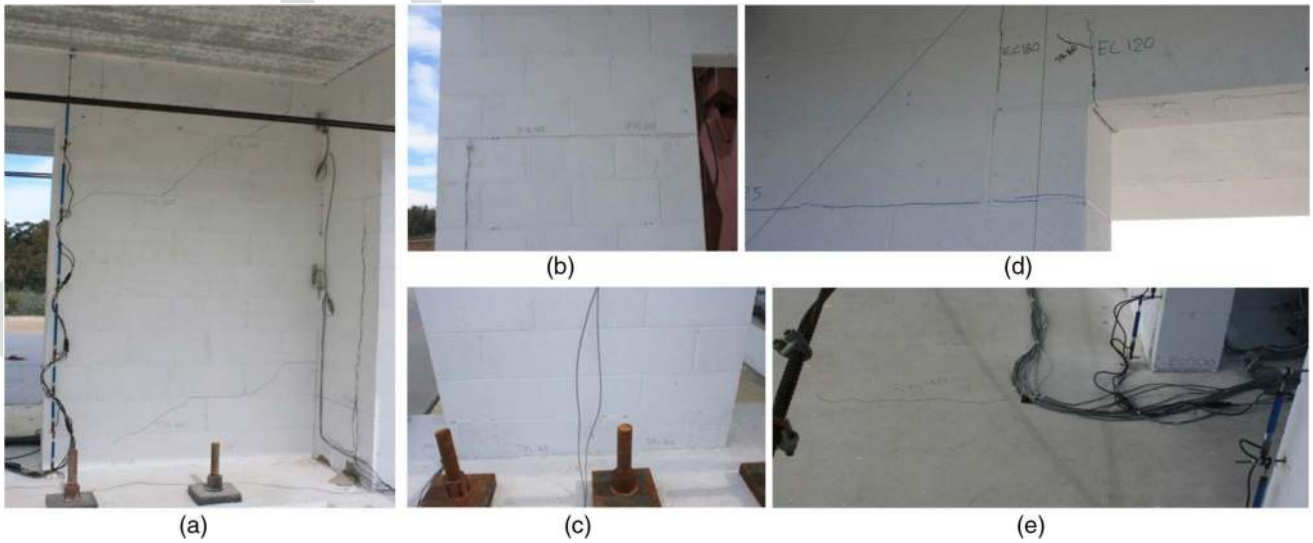

F8:1 **Fig. 8.** Cracks in the first and second stories after syl160: (a) diagonal cracks in W-3; (b) tensile cracks at the top of W-4; (c) tensile cracks at the
F8:2 bottom of W-4; (d) cracks at control joint at the top of W-2 in the second story; and (e) cracks in second-floor slab

that stain gages were installed only at the extreme bars and near the bottom of the walls in the second story. Moreover, the yielding of the extreme vertical bars in W-1 and W-3 in the bottom story propagated to the third masonry course from the base.

150% of Chi Chi

The last two tests with 150% of the Chi Chi record (chi150a and chi150b), were severe. As shown in Fig. 6(b) and Table 7, within the period range of the damaged structure, both tests had spectral intensities significantly higher than the MCE. Even though the input motions were identical in the two tests, the motions recorded on the table were different due to the change of the structural stiffness, which affected the table-structure interaction.

During chi150a, severe diagonal cracks developed in the two T-walls in the bottom story. The maximum residual crack width after the test was approximately 1.5 mm (0.06 in.). The maximum bottom-story drift measured during the test was 0.73% as the maximum relative displacement between the foundation and the first slab was 19.7 mm (0.78 in.). In W-2, 13.5 mm (0.53 in.) of the total drift was contributed by base sliding. Due to the damage, the fundamental period of the structure increased from 0.22 to 0.25 s. The strain gages indicate that a large number of the bars in the three in-plane walls yielded during this test [Fig. 5(a)]. The gages indicating yielding include gages placed on horizontal bars at the mid-height of the walls as well as a horizontal bar crossing the control joint between wall W-1 and the lintel beam. More gages indicated yielding for the first time than any other test.

During chi150b, the structure was severely damaged. The shear cracks in the T-walls in the bottom story were severe with a maximum residual width of approximately 10 mm (0.4 in.). The final damage pattern is shown in Fig. 9. Fig. 9(c) shows that the horizontal bar at the bottom of wall W-3 was still functional despite the severe toe crushing and spalling because of the 180° hook. Wall W-2 had only two noticeable horizontal cracks; one at its base and one in the bed joint right below the level of the top of the door openings. The base sliding of this wall exceeded 25.4 mm (1 in.), which was the maximum range of the LVDTs used to measure sliding. Moreover, the dowels at the base were sheared off, as confirmed during the demolition of the structure after the testing. Walls W-1 and W-3 slid considerably less, as indicated in Table 7. Although chi150a was more demanding than chi150b, the story drift measured during chi150b was significantly larger with a maximum drift ratio of 1.59%, while that during chi150a was 0.74%. This also resulted in some additional gages indicating yielding in the vertical and horizontal bars of walls W-1, W-3, and W-4.

Evaluation of Test Results

Deformation Mechanisms

Fig. 10 compares the displacements at the top of the in-plane walls (W-1, W-2, and W-3) in the first story due to flexure to the total displacement for different ground-motion levels. The flexure-related displacement of each wall is calculated by integrating the wall curvatures over the distance between the top of the foundation and the bottom of the slab in the second level. The curvature is determined for each wall from the readings of the displacement transducers mounted along its edges as shown in Fig. 4, and it is assumed to be constant over the gage length of each pair of displacement transducers. Fig. 10 shows that in ec180, the three walls had almost the same flexural deformation, which accounts for about 70% of the total first-story displacement. The rest of the wall deformation was mainly due to shear, and a small portion was caused by base sliding, the peak values of which are shown in Table 7. In ec250, the flexural deformation of W-2 started to deviate from that of W-1 and W-3 after 17 s. After that point, the contribution of base sliding to the displacement between the top and base of W-2 increased, as shown in Table 7. The deformed shape of the bottom story of the structure at the peak story drift in ec250, as constructed from the readings of the displacement transducers, is shown in Fig. 11. The figure shows that the west T-wall had horizontal flexural cracks at the top and bottom due to rocking, while wall W-2, which started to slide more significantly at the base, had a relatively small flexural crack at the base and separated from the lintel beams due to the opening of the control joints. The east T-wall was under high compression and did not develop significant cracks.

In chi100, the contribution of the flexural deformation of W-2 dropped to 20% of the total displacement as shown in Fig. 10(c), due to severe base sliding. In this test, the flexural deformations of W-1 and W-3 accounted for 50% of the total displacement, with

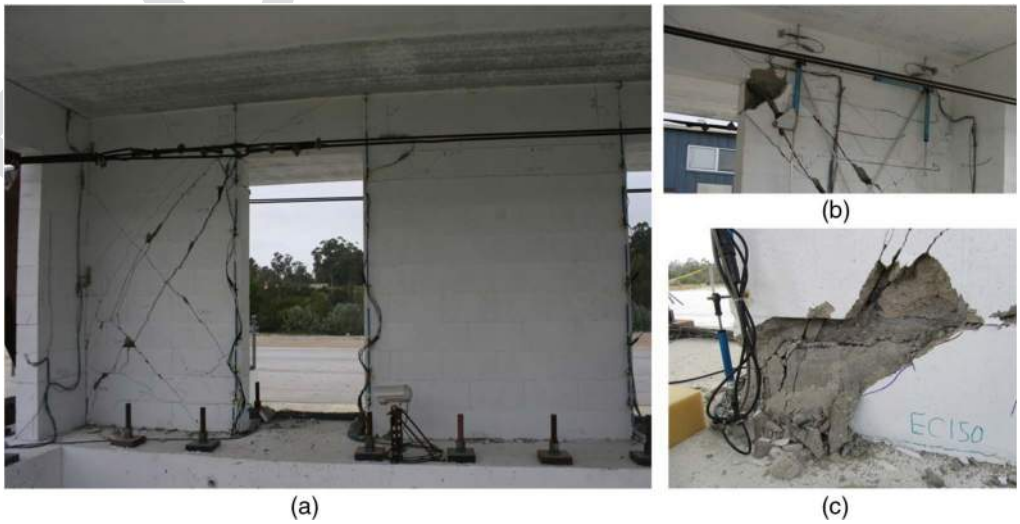

Fig. 9. Damage of first-story walls at the end of testing: (a) W-1 and W-2 after completion of the tests; (b) spalling at the top of W-1; and (c) spalling at the toe of W-3, exposing hook of horizontal bar

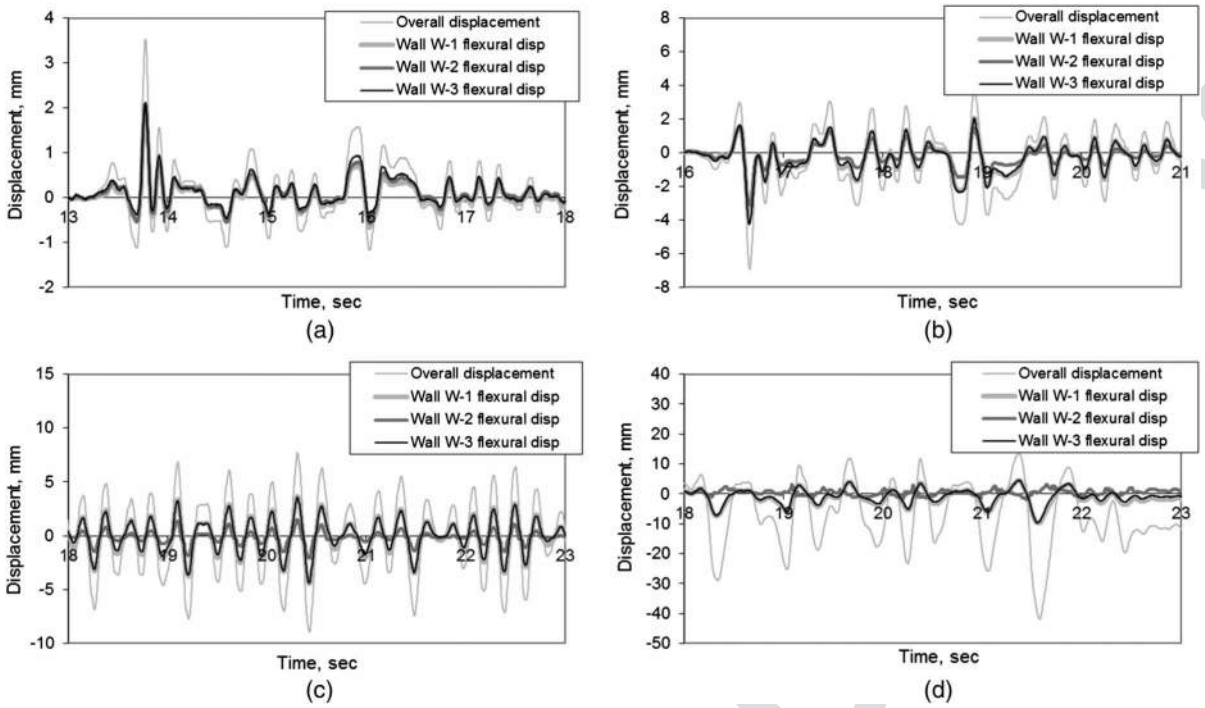

F10:1 **Fig. 10.** Total and flexural deformations of W-1, W-2, and W- 3 in the first story: (a) ec180; (b) ec250; (c) chi100; and (d) chi150b

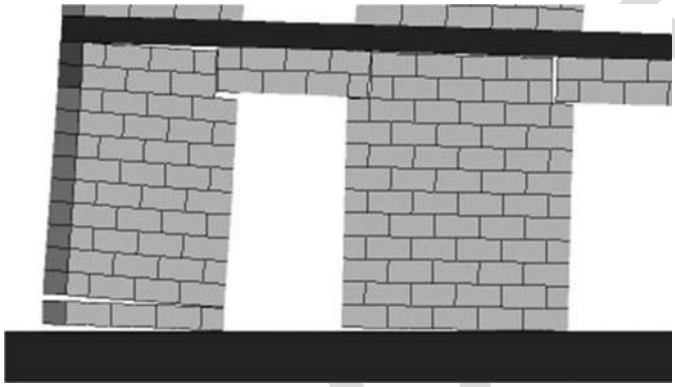

F11:1 **Fig. 11.** Deformed shape of Walls W-1 and W-2 at peak base shear
F11:2 for ec250

shear deformation accounting for most of the rest. In chi150 b, the contribution of flexural deformation to the total displacement decreased significantly for all walls. For W-1 and W-3, this decrease was caused by the opening of major diagonal shear cracks, which first developed in chi150a.

The tensile strains in the horizontal bars at the mid-height of W-1 and W-3 were below the yield strain prior to chi150a, but exceeded the yield strain in chi150a due to the occurrence of major diagonal shear cracks in the walls. Fig. 12 shows the tensile strains in the middle of the horizontal bars at mid-height of W-1 and W-3 versus first-story drift for chi150a. The west wall (W-1) developed higher tensile strain when the structure displaced toward the west (negative) direction, while the east wall (W-3) developed higher tensile strain when the structure displaced toward the east (positive) direction. This can be attributed partly to the fact that the exterior wall on the side towards which the structure deformed (i.e., wall W-1 for negative drifts and wall W-3 for positive drifts) sustained

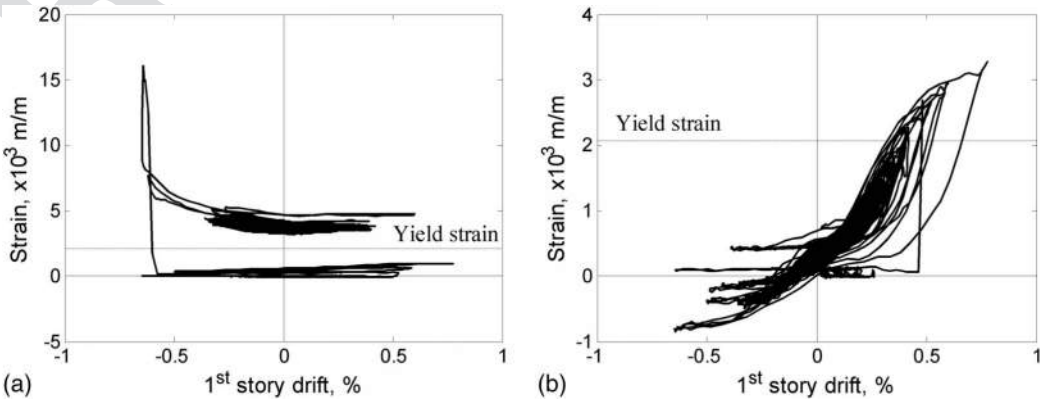

F12:1 **Fig. 12.** Strains in horizontal shear reinforcement at mid-height of bottom-story walls in chi150a: (a) Wall W-1; and (b) Wall W-3

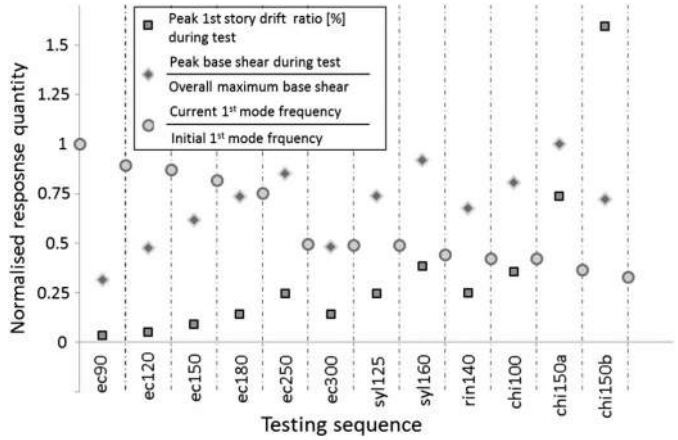

F13:1 **Fig. 13.** Normalized peak response values and 1st mode frequency

most of the seismic shear because it was subjected to a higher compression due to the overturning moment acting on the entire wall system. This dependence of the strain in the shear reinforcement on the loading direction can also be partly attributed to the fact that the flange restrained the opening of the diagonal crack running from the upper corner of the wall web near the flange to the web toe on the opposite side. Restraining this diagonal crack opening reduced the tension demand on the horizontal shear reinforcement. As shown in Fig. 12, the maximum tensile strain developed in W-1 was significantly larger than that in W-3 and was approximately 7.5 times the yield strain. The same tendency is observed for chi150 b with the maximum tensile strains in the horizontal bars slightly reduced, which could be attributed to the bond deterioration and slip of the horizontal bars.

Base Shear, First-Story Drift and Fundamental Frequency

Fig. 13 presents the peak first-story drift ratio and normalized peak base shear measured in each seismic test, and the ratio of the fundamental frequency of the structure after each seismic test to the fundamental frequency of the intact structure before the first seismic test. The base shear is normalized by the maximum value reached in the entire testing sequence, which occurred in chi150a. One can note that the structure developed the highest base shear in ec250, syl160, and chi150a. In ec250, the base shear reached 85% of the maximum value, and the fundamental frequency had the most significant drop for the entire test program. The first-story drift increased significantly in chi150a and chi150 b. The substantial increase of the peak bottom-story drift, together with the significant drop of the peak base shear in chi150 b, indicate that the structure suffered severe damage, which is consistent with the severity of shear cracks observed in walls W-1 and W-3. Interestingly, the observed change of the fundamental frequency was not significant after this test. This is probably due to the relatively low amplitude of the white-noise excitation, which did not induce sufficient displacement to detect the severe stiffness degradation that had occurred.

The plot of base shear versus first-story drift is presented in Fig. 14. The base shear is normalized with respect to the seismic weight of the test structure, which was 923.9 kN (207.9 kips). The figure indicates that the resistances in the two directions were quite different despite the fact that the structure was symmetric. The maximum base shear developed in the negative direction was 2.03 times the seismic weight of the test structure, while in the positive direction the strength was 25% lower than the peak strength in the negative direction. The difference in the resistances in the two directions can be attributed to the different locations of lap splices in the vertical reinforcement of the two T-walls as discussed in a following section. As shown in Fig. 14, the envelope of the response in the positive direction resembles an elastic-plastic behavior. The peak shear force in this direction was reached in ec180 at a drift of 0.14%. In six of the subsequent tests, the structure reached at least 90% of this base shear but did not exceed it although the maximum drift reached 0.74%. The structure exhibited a different behavior in the negative direction in which the peak strength was 33% higher but was followed by significant strength degradation when the drift ratio exceeded 0.60%. This relatively brittle behavior is consistent with results of quasi-static tests conducted on shear-critical wall segments (Ahmadi et al. 2012). A flexure-dominated special reinforced masonry wall should be able to sustain a story drift of more than 1% without severe strength degradation. Despite the shear-dominated mechanism, the structure performed satisfactorily as it withstood nine tests with intensities exceeding the MCE.

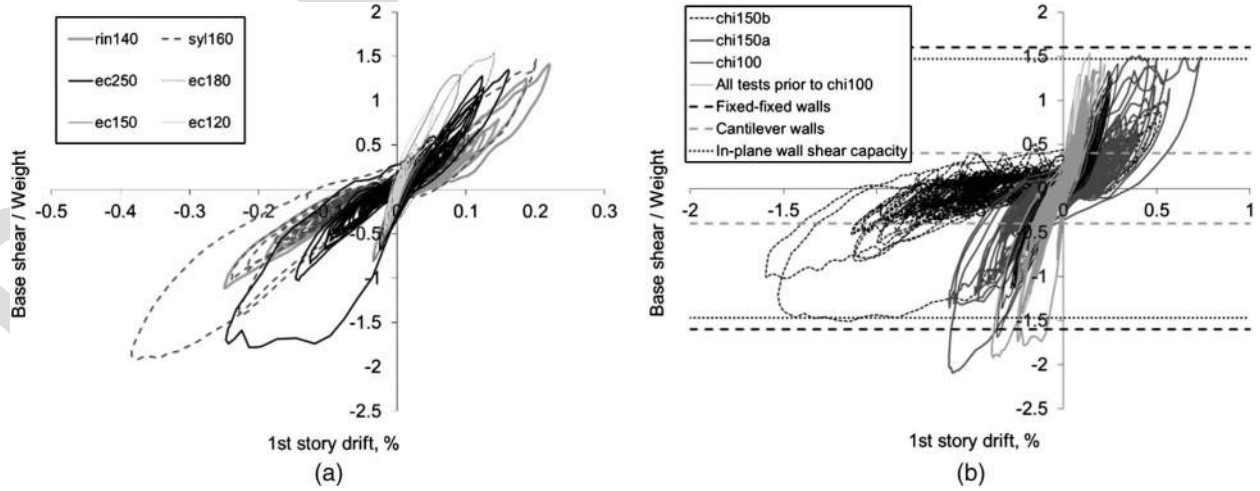

F14:1 F14:2 **Fig. 14.** Base shear versus first-story drift: (a) base shear versus first-story drift for selected tests; and (b) base shear versus first-story drift for the last three tests

Coupling Actions of Horizontal Diaphragms and Lintels

In the positive (weak) direction, the ratio of the base-shear capacity developed by the structure to the seismic weight of 1,024 kN (230 kips) considered in the design was 1.35, while the design base-shear coefficient (C_S) was only 0.2. Hence, the actual base-shear capacity of the structure was 6.75 times the design base shear. The significant over-strength exhibited by the test structure and the shear-dominated behavior of W-1 and W-3 in chi150a and chi150 b can be attributed to the coupling actions exerted by the horizontal diaphragms and the lintels. Even though the horizontal reinforcing bars in the lintels were debonded, the lintels were still able to cause a diagonal strut action. To assess the extent of the coupling actions, the theoretical base-shear capacities of the wall system associated with the flexural mechanism are computed for two limiting scenarios using the actual strengths of the reinforcing steel and masonry prisms shown in Tables 1 and 5, respectively. The first scenario ignores the coupling actions, treating all three in-plane walls as cantilever walls as assumed in the design. The second has rigid coupling elements, with the top and the base of the walls in each story fixed against rotation. In this calculation the top of each wall is considered to be at the level of the door opening (i.e., the wall is two courses shorter than the floor height) assuming that the lintels are rigid. The second scenario provides the upper-bound capacity.

Even though a coupled wall system will have additional axial forces introduced in the wall elements due to the overturning moment caused by the lateral forces, the influence of these axial forces on the moment capacity of the walls is ignored. This is a reasonable assumption because the axial compression introduced in one of the two outer walls will approximately offset the effect of the axial tension introduced in the other, and the coupling actions on the two sides of the center wall (W-2) will cancel each other.

The calculated base-shear capacities are shown in Fig. 14(b). It can be seen that the capacity of the test structure far exceededs the flexural capacity calculated for cantilever walls, and the resistance developed in the strong (negative) direction exceeds that calculated with the fixed-fixed end conditions (rigid coupling element assumption) by 26%. This indicates that the walls behaved more like a system with rigid coupling elements. The overstrength observed in the strong direction can be attributed to the resistance provided by the out-of-plane walls as discussed later.

The existence of strong coupling actions is consistent with the deformed shape and crack pattern of the wall system shown in Fig. 11, which shows that the T-wall deformed with a combination of rocking and bending in double curvature. It is also confirmed by the strains in the vertical reinforcement measured near the top and the base of each wall in the bottom story and the wall curvatures measured by displacement transducers. Fig. 15(a) shows the strains in the extreme east vertical bar in the web of the west T-wall (W-1) plotted against the story drift for ec250. The figure shows that tensile strain developed near the top of the wall (at the height of the door openings) and compressive strain developed at the base when the structure displaced toward the east (the positive direction). The signs of the strains were reversed when the wall displaced toward the west. This indicates that the wall was subjected to double curvature because of the strong coupling action. Fig. 15(b) shows the curvatures at the top and bottom of W-1 plotted against the first-story drift for ec250. The curvatures are calculated from the readings of displacement transducers over a 406 mm (16 in.) gage length centered at elevations 406 mm below the top of the door openings and 406 mm above the base of the wall, respectively. The locations of these sensors are indicated by shaded ellipses in Fig. 4. The curvature is positive when the flange of the wall is in compression. Although the wall was in double curvature, the curvature developed near the base of the wall was far larger than that at the level of the bottom of the lintel beam. This indicates that even though there was a strong coupling action, the top of the wall was not perfectly fixed against rotation by the lintel. It should be noted that if the entire height of the wall between the slabs is considered, the curvature closer to the top of the wall would be larger but still lower than the curvature at the base of the wall.

Only hairline cracks were observed on the top of the horizontal diaphragms as shown in Fig. 8(e). The strains measured in the reinforcing bars parallel to the in-plane walls in the topping of the horizontal diaphragm at the second-level show that a bar at a distance of 610 mm (24 in.) from the center line of the in-plane walls had a maximum tensile strain of 2.5×10^{-3} in ec250, which is slightly above the yield strain. In all subsequent tests, the strain in that bar dropped below 60% of the yield strain. The next bar, at a distance of 1,016 mm (40 in.) from the in-plane walls had a maximum strain of 1.2×10^{-3} recorded during the entire test program. This indicates that the slabs were very stiff and strong and did not deform significantly.

Influence of Lap Splices

In the bottom story, the vertical reinforcement in W-1 (west wall) had lap splices at the mid-height of the story, while in W-3 (east wall), it had lap splices at the base. Fig. 16(a) compares the strains

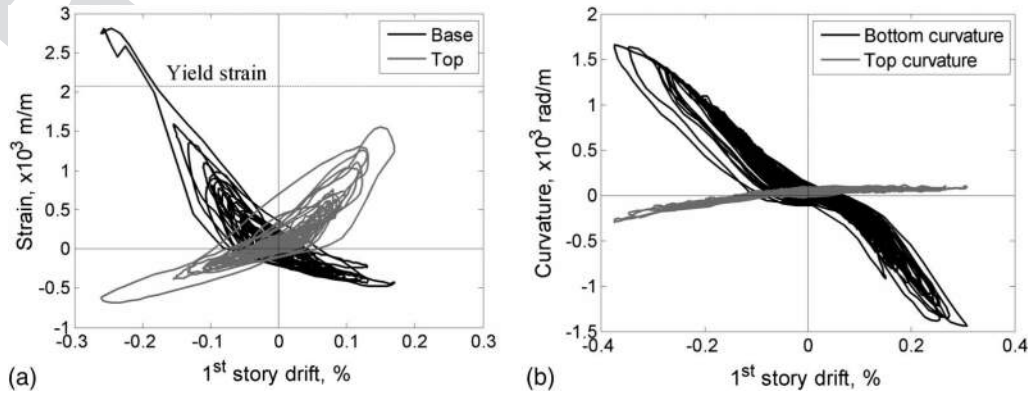

Fig. 15. Bar strains and wall curvatures for W-1 during ec250: (a) strains in the vertical bar next to the first-story door opening; and (b) curvatures in W-1 in the first-story

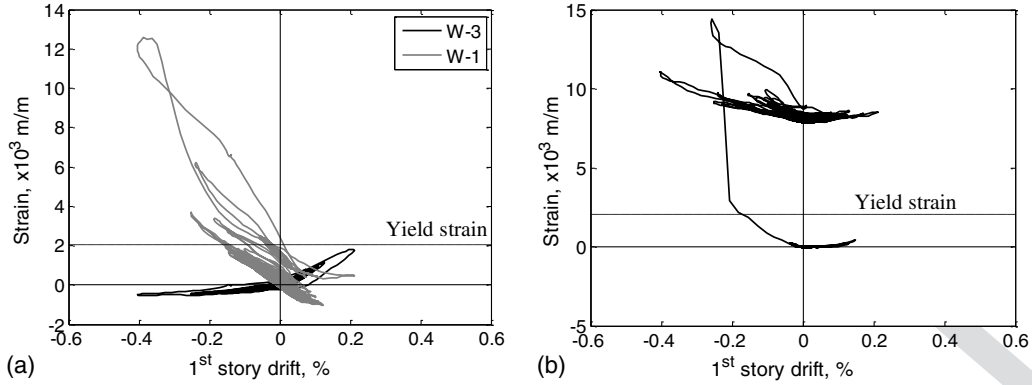

F16:1 F16:2 **Fig. 16.** Strains on vertical bars during syl160: (a) vertical bar strains near the first-story door openings at the base of walls W-1 and W-3; and (b) vertical bar strain near the base of wall W-7

developed in the vertical bars at the base of W-1 and W-3 next to the door openings during syl160. It can be seen that the tensile strain developed at the base of W-1 at 0.2% drift in the negative direction was around 6×10^3 m/m, while that for W-3 at the same drift level in the opposite direction is much smaller (by a factor of 3). It should be noted that the magnitudes of base sliding in the two walls were comparable as shown in Table 7. The smaller tensile strain measured in W-3 can be attributed to the slip of the dowel bar in the lap splice. The slip of the dowel bar compromised the flexural strength of W-3. The lower flexural strength resulted in a lower shear demand on W-3. This is supported by the fact that the maximum tensile strain developed in the horizontal reinforcement in W-3 during chi150a was much lower than that in W-1, as shown in Fig. 12. This explanation is also consistent with the fact that the wall system exhibited a lower resistance when the structure displaced in the positive (east) direction as shown in Fig. 14. Wall W-3 had a more significant contribution to the lateral resistance in the positive direction as compared to that in the negative direction because the wall was under a higher axial compression when displaced in the positive direction.

Tests by Sherman (2011) on planar-reinforced masonry cantilever wall segments have shown that the presence of lap splices at the base could jeopardize the ductility and post-peak behavior of a wall but not its flexural strength. The reduction of the flexural strength of W-3 could be attributed to the flange effect of the T-wall, which resulted in more tension demand on the extreme vertical bar in the web. This effect could also be exacerbated by the repeated shaking of the structure during the shake-table tests.

Influence of Out-Of-Plane Walls

Fig. 14(b) shows that the lateral resistance of the structure in the negative drift direction was 26% higher than the theoretical resistance of the in-plane walls with fixed-fixed end conditions in each story, even though in reality the walls were not completely fixed at the top. This overstrength can be partly attributed to the out-of-plane walls. The out-of-plane walls (W-4, W-6, W-7, and W-9) increased the lateral resistance of the structure in two ways. One is the out-of-plane bending of these walls. The second and more important factor is the restraining effect exerted by these walls on the rocking of the in-plane walls. The strain-gage data indicate that the vertical reinforcement in the out-of-plane walls yielded very early, as shown in Fig. 4(b) and developed high tensile strains throughout the tests. The tension in the out-of-plane walls exerted an axial compression on the in-plane walls through the stiff horizontal diaphragm when the latter rocked after flexural cracks developed at the top and the base. The additional axial compression increased the flexural resistance of the in-plane walls.

Fig. 16(b) shows the strain developed in a vertical reinforcing bar at the base of W-7. It can be seen that the bar was always subjected to tension, and the tensile strain increased as the structure displaced toward the east (positive direction) and the west (negative direction). This is due to the axial extension of the in-plane walls as

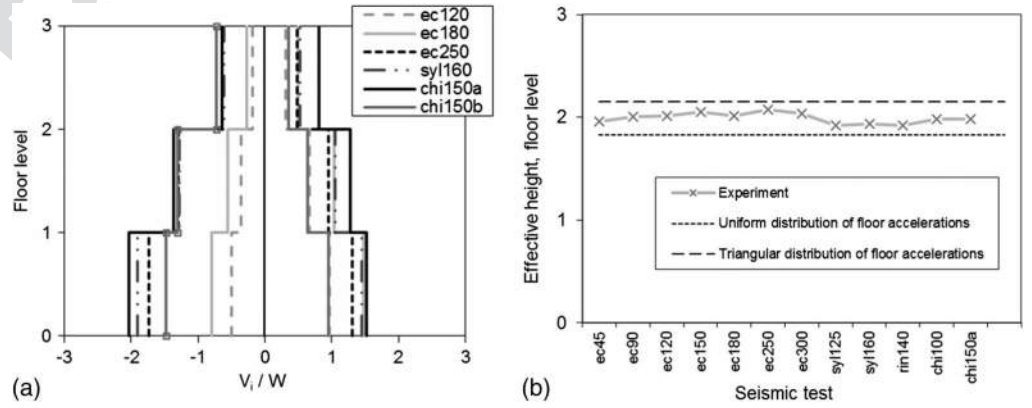

F17:1 F17:2 **Fig. 17.** Story shears and effective height of lateral-force resultant: (a) normalized peak story shear forces; and (b) effective height of resultant lateral force

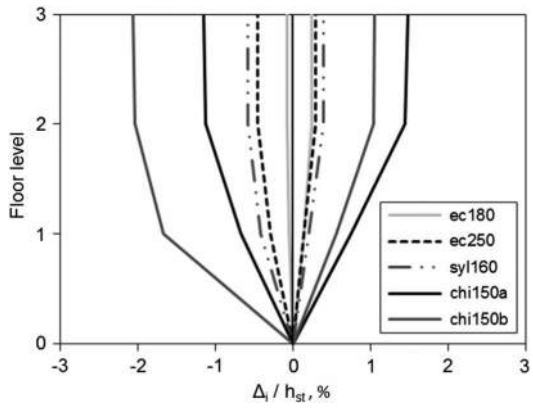

F18:1 **Fig. 18.** Normalized displacements in each story (h_{st} is the story
F18:2 height)

they rocked. However, the strain plot shows some directional bias in that the increase in tensile strain in W-7 was more significant when the structure displaced toward the west (the negative direction). This was caused by the overturning moment acting on the structure. The quantification of the exact contribution of the out-of-plane walls to the lateral resistance of the structure requires further studies using computational models.

Distribution of Story Shear and Story Drifts

The distribution of peak shear force normalized by the seismic weight of the test structure in each story is shown in Fig. 17(a) for the four most important tests (ec250, syl160, chi150a, and chi150b), and also for ec120 and ec180, in which the structure had little or no damage. The distribution of the inertia forces over the height permits the determination of the effective height of the resultant lateral force, which is calculated for each test as the ratio of the peak overturning moment at the base to the peak base shear. As shown in Fig. 17(b), initially the effective height was close to the height of the resultant force corresponding to a triangular load distribution. However, it became closer to that corresponding to a uniform load distribution after ec250 as the damage in the bottom story increased. The profiles of the peak floor displacements normalized by the story height are shown in Fig. 18.

Conclusions

This paper presents the shake-table tests of a full-scale, 3-story, special reinforced masonry wall system designed according to current code provisions and practice. The structure was designed as a cantilever wall system by ignoring the coupling actions of the horizontal diaphragms and the lintels. It was subjected to a sequence of 14 scaled earthquake ground motion records, nine of which exceeded the MCE considered in the design.

Even though the lintels above door openings were separated from the vertical wall elements by control joints, the horizontal diaphragms and the lintels exerted strong coupling forces and moments on the wall elements. As a result, the final failure mechanism was dominated by diagonal shear cracks in the two outer T-walls in the bottom story and by sliding at the base of the in-plane lineal wall. This led to a soft-story mechanism and severe strength degradation in one loading direction after the drift in the first story exceeded 0.6%. This, however, occurred after the flexural reinforcement in the T-walls had developed severe tensile yielding.

In spite of the shear-dominated mechanism, the structure performed satisfactorily as it withstood nine earthquake ground motions with intensities exceeding the MCE. The actual base-shear capacity of the structure was much higher than that expected of a cantilever wall system, reaching 6.75 times the design base shear. This high overstrength is attributed primarily to the coupling actions of the horizontal diaphragms and the lintels, which were ignored during the design. The out-of-plane walls also contributed to the lateral resistance of the structure by exerting axial compression on the in-plane walls. The good performance of the structure can also be attributed to the quantity of shear reinforcement in the walls, which was governed by the prescriptive spacing requirement of the code and the use of 180-degree hooks for the shear steel. The lower lateral load resistance of the structure in one loading direction can be attributed to the presence of lap splices near the base of one of the two T-walls. This, together with the strain data obtained from the walls, provides evidence that lap splices in the plastic-hinge region of a wall could compromise its flexural capacity.

Acknowledgments

This study was supported by a NIST ARRA Measurement Science and Engineering Grant awarded to the University of California at San Diego under Award No. 60NANB10D013. The shake-table tests were conducted with the support of the Network for Earthquake Engineering Simulation Program of NSF. The third author would also like to acknowledge a Graduate Fellowship from UC, San Diego, which partially supported his graduate studies. The technical assistance and support of the staff at the Englekirk Structural Engineering Center of UC, San Diego in the shake-table tests is greatly appreciated. Finally, the authors would like to thank Dr. Matthew Schoettler for his assistance in post-processing the test data. The opinions expressed in this paper are those of the authors and do not necessarily represent those of the sponsors.

References

Abrams, D., and Paulson, T. (1991). "Modeling earthquake response of concrete masonry building structures." *ACI Struct. J.*, 88(4), 475–485.

Ahmadi, F. (2012). "Displacement-based Seismic Design and Tools for Reinforced Masonry Shear-wall Structures." Ph.D. dissertation, Univ. of Texas, Austin, TX.

ASCE/SEI. (2005). "Minimum design loads for buildings and other structures." Reston, VA.

ASCE/SEI. (2010). "Minimum design loads for buildings and other structures." Reston, VA.

Assis, G. F., Hamid, A. A., and Harry, H. G. (1989). "Material models for grouted block masonry." *Rep. No. 1.2(a)-2*, U.S.-Japan Coordinated Program for Masonry Building Research, Drexel Univ., Philadelphia.

ASTM. (2006). "ASTM volume 04.05 chemical-resistant nonmetallic materials; vitrified clay pipe; concrete pipe; fiber-reinforced cement products; mortars and grouts; masonry; precast concrete." West Conshohocken, PA.

Bozorgnia, Y., and Bertero, V. (2004). *Earthquake engineering: From engineering seismology to performance-based engineering*, CRC Press LLC, Boca Raton, FL.

Cohen, G. L., Klingner, R. E., Hayes, J. R., Jr., and Sweeney, S. (2004a). "Seismic response of low-rise masonry buildings with flexible roof diaphragms. Part I: Seismic and quasi-static testing." *EERI Spectra, Earthquake Eng. Res. Inst.*, 20(3), 779–801.

Cohen, G. L., Klingner, R. E., Hayes, J. R., Jr., and Sweeney, S. (2004b). "Seismic response of low-rise masonry buildings with flexible roof diaphragms. Part II: Analytical modeling." *EERI Spectra, Earthquake Eng. Res. Inst.*, 20(3), 803–824.

Gulkan, P., Clough, R. W., Mayes, R. L., and Manos, G. (1990a), "Seismic testing of single-story masonry houses. Part I." *J. Struct. Eng.*, 10.1061/(ASCE)0733-9445(1990)116:1(235), 235–256.

Gulkan, P., Clough, R. W., Mayes, R. L., and Manos, G. (1990b). "Seismic testing of single-story masonry houses. Part II." *J. Struct. Eng.*, 10.1061/(ASCE)0733-9445(1990)116:1(235), 235–256.

Klingner, R. E., Shing, P. B., McGinley, W. M., McLean, D. I., Okail, H., and Jo, S. (2010). "Seismic performance tests of masonry and masonry veneer." *J. ASTM Int.*, 7(3), 102740.

Leiva, G., and Klingner, R. E. (1994). "Behavior and design of multi-story masonry walls under in-plane seismic loading." *Masonry Soc. J.*, 13(1), 15–24.

Masonry Standard Joint Committee. (2008). "Building code requirements for masonry structures." *TMS 402-08/ACI 530-08/ASCE 5-08*, The Masonry Society, Boulder, CO.

Masonry Standard Joint Committee. (2011). "Building code requirements for masonry structures." *TMS 402-11/ACI 530-11/ASCE 5-11*, The Masonry Society, Boulder, CO.

Mojiri, S., El-Dakhakhni, W. W., and Tai, M. J. (2014). "Shake table seismic performance assessment of lightly reinforced concrete block shear walls." *J. Struct. Eng.*, 04014105.

Priestley, M. J. N. (1993). "Seismic design of concrete masonry shear-walls." *ACI Struct. J.*, 83(1), 58–68.

Sayah, A., Stavridis, A., Sherman, J., and McLean, D. (2013). "Finite element modeling of reinforced masonry shear walls under seismic loads." *12th Canadian Masonry Symp.*, Vancouver, Canada.

Seible, F., Hegemier, A., Igarashi, A., and Kingsley, G. (1994a). "Simulated seismic-load tests on full-scale five-story masonry building." *J. Struct. Eng.*, 10.1061/(ASCE)0733-9445(1994)120:3(903), 903–924.

Seible, F., Priestley, N., Kingsley, G., and Kurkchubashe, A. (1994b). "Seismic response of full-scale five-story reinforced-masonry building." *J. Struct. Eng.*, 10.1061/(ASCE)0733-9445(1994)120:3(925), 925–946.

Sherman, J. D. (2011). "Effects of key parameters on the performance of concrete masonry shear walls under in-plane loading." Master thesis, Dept. of Civil and Environmental Engineering, Washington State Univ., Pullman, WA.

Shing, P. B., Schuller, M., Hoskere, V. S., and Carter, E. (1990). "Flexural and shear response of reinforced masonry walls." *ACI Struct. J.*, 87(6), 646–656.

Stavridis, A., Koutromanos, I., and Shing, P. B. (2012). "Shake-table tests of a three-story reinforced concrete frame with masonry infill walls." *J. Earthquake Eng. Struct. Dyn.*, 41(6), 1089–1108.

Stavridis, A., Mavros, M., and Shing, B. (2013). "Shake-table testing of a 3-story, full-scale, reinforced masonry wall system." Network for Earthquake Engineering Simulation (database), Dataset.

Yousefianmoghadam, S., Behmanesh, I., Stavridis, A., Moaveni, B., and Nigbor, R. L. (2014). "System identification of a ten-story RC building at different damage states." *Engineering Mechanics Institute Conf.*, ASCE, Hamilton, Canada.